J. Synchrotron Rad. (1999). **6**, 1059–1064

Uranium-sensitive tomography with synchrotron radiation

Th. Materna,[a]* J. Jolie,[a] W. Mondelaers,[b] B. Masschaele,[b] V. Honkimäki,[c] A. Koch[c] and Th. Tschentscher[c,d]

[a]Institute of Physics, University of Fribourg, Pérolles, CH-1700 Fribourg, Switzerland, [b]Department of Subatomic and Radiation Physics, University of Ghent, Proeftuinstraat 86, B-9000 Ghent, Belgium, [c]European Synchrotron Radiation Facility, BP 220, F-38043 Grenoble CEDEX, France, and [d]Hamburger Synchrotronstrahlungslabor HASYLAB at Deutsches Elektonesynchrotron DESY, Notkestrasse 85, D-22603 Hamburg, Germany. E-mail: thomas.materna@unifr.ch

(*Received 21 April 1999; accepted 22 June 1999*)

Element-sensitive tomography produces quality information in the field of medical imaging. This method, also known as dichromatic tomography, can be useful to visualize the distribution of heavy elements, such as actinides, without destroying the sample. One of the problems is to obtain a monochromatic photon beam of sufficiently high energy; the other is to have a way of recording these high-energy photons with a good spatial resolution. Here, the results of a first experiment on uranium mapping with synchrotron radiation are reported. Various natural and artificial samples of a few centimetres in size with uranium concentration between 0.008 g cm^{-3} and 2 g cm^{-3} were scanned using photon beams around 115 keV and a specially designed camera. The data were then analysed using a conventional fast reconstruction technique. This yielded excellent results with spatial resolutions down to 50 μm. For the first time it was shown that element-sensitive tomography using synchrotron radiation could be extended to the heaviest natural element. Therefore, in principle, the spatial distribution of any element can now be reconstructed using synchrotron radiation. Extension of this technique to very heavy elements can be important for geology, health physics and nuclear waste storage.

Keywords: tomography; *K*-edge; non-destructive analysis; high-energy synchrotron radiation; uranium; imaging; CCD camera.

1. Introduction and concept

What makes element-sensitive tomography so attractive is the simplicity of the method from the analytical point of view. By imaging a sample using X-ray photons having two different energies, one just below and one just above the *K*-edge energy of the element of interest, the ratio of the images become sensitive to this element only (Lewis, 1997; Grodzins, 1983; Fryar *et al.*, 1987). The *K*-edge causes an abrupt increase of absorption of photons by an element. It occurs when photons have enough energy to ionize the innermost electrons of an atom. A standard procedure for a tomographic scan is to measure the attenuation at several orientations of the sample. The recorded patterns are then used to reconstruct the three-dimensional attenuation distribution for the whole sample. If the ratios of the images taken right above and below the *K*-edge are used as input, the reconstruction yields only the spatial distribution of the element under study.

The *K*-edge energies are different for each element. It is therefore possible to visualize independently the distribution of different elements, inside the same sample, by tuning the energy. This property can be of great interest in geology and nuclear waste storage, by studying selectively the spatial distribution of radioactive elements and their daughters produced by disintegration. But the technique can also be linked to other fields including medicine or research and development for industry. Indeed, heavy elements are sometimes used as coatings (Au, W); therefore, visualizing the coating itself or the diffusion of the element inside the coated piece leads to other studies. Another application of this technique is the study of filters for heavy elements (Pb, U).

Another property of the element-sensitive tomography is that partial scans using non-compact supports having dimensions larger than the image size become possible: if only a part of the object contains the element under study, this part alone will give a signal in the ratio images and has to be scanned. Therefore, it is not necessary to scan the whole object, because the absorption in the other parts is equal at both energies. This holds only when the absorption in the outer part is not too strongly lowering the statistics. This property opens opportunities for the study of large objects if the heavy element is localized. Zooming in on the part of interest should also be possible in this case.

When heavy elements, such as actinides, are of interest, the photon energies required are above 100 keV. The high energy of these photons, leading to a large penetration depth, permits the use of thick and dense samples. On the other hand, there are two disadvantages: it is difficult to produce tunable sources of photons above 100 keV and, because of their strong penetration, these photons are also difficult to record. Here we show how these problems associated with heavy-element tomography can be overcome. Our approach relies on synchrotron radiation above 100 keV and a position-sensitive detector capable of working at these energies.

2. Experimental procedure

Nowadays, several groups around the world work with synchrotron radiation on medical or material tomography, including absorption tomography or phase-contrast tomography (Bonse *et al.*, 1996; Flannery *et al.*, 1987; Kinney *et al.*, 1994; Snigirev *et al.*, 1995). Beamlines have also been dedicated to these techniques at the ESRF (medical beamline, imaging diffraction), NSLS (microtomography) *etc*. However, few of them use high-energy photons.

Our earlier work on heavy-element detection relied on crystal diffraction of bremsstrahlung to provide the incident beam and semiconductor detectors for the detection (Bertschy *et al.*, 1995). Because of limited source intensity and detector sensitivity, these studies yielded only integrated two-dimensional distribution maps (Bertschy *et al.*, 1996; Materna *et al.*, 1999). The tremendous improvements in synchrotron radiation as provided at the ESRF (Tschentscher & Suortti, 1998) allowed the transfer of the technique to photon beams with intensities that are several orders of magnitudes higher.

For the high-energy tomography set-up at beamline ID15a of the ESRF, illustrated in Fig. 1, a superconducting wavelength shifter was chosen to produce the X-ray beam. It consists of three consecutive dipole magnets with alternating fields, which serve to create a wiggle in the electron trajectory. Because this device is superconducting, it is possible to have a high magnetic field (4 T) acting on the electrons, implying high-energy X-ray photons (from 30 keV to 1000 keV, the critical energy being 100 keV). About 60 m from the source, two bent asymmetric-cut Si crystals working in fixed Laue–Laue mode selected the correct energy. Asymmetric-cut crystals are used to enlarge the crystal reflectivity curve. It increases the integral reflectivity and thus the photon intensity but at the cost of degrading the energy resolution (Nave *et al.*, 1995). Two energies close to the *K*-edge of uranium were chosen to perform the tomographies: 114.6 and 116.6 keV with an energy resolution of 250 eV. Between these two energies the attenuation coefficient in uranium differs by a factor of 3.3 (μ/ρ = 1.4 cm^2 g^{-1} at 114.6 keV, μ/ρ = 4.6 cm^2 g^{-1} at 116.6 keV), whereas for other elements the difference is negligible (for example, the attenuation coefficient in lead decreases by 4% only).

The monochromatic beam then passed through a vacuum tube in order to avoid scattering of X-rays by air before reaching the sample, which was placed on a rotation table. Finally, the detection system was placed at the end of the set-up to record the absorption image of the sample. At the sample position a parallel beam with a reasonable homogeneity was obtained over a 5 mm-high and 20 mm-wide surface. The variation of intensity attained 20% in the horizontal direction and 50% in the vertical direction. To avoid artefacts due to this slight variation, all images were normalized before treatment. The intensity of the beam at the sample was of the order of 10^8 photons s^{-1} mm^{-2}.

A new detection system had to be developed, because traditional γ-ray detectors cannot operate with such high intensities. Since the detector, preferentially, should be able to handle high counting rates combined with a high spatial resolution, we opted for a powder phosphor screen consisting of an 80 µm-thick Gd_2O_2S:Tb layer. The screen was imaged using a 1:1 optical lens, a 45° mirror and a CCD camera. The mirror was used to keep the camera out of the direct beam. The CCD had a sensitive area of 24.6 × 24.6 mm^2 covered by 1024 × 1024 pixels, a dynamic range of 14 bits (16384 grey levels per pixel) and was cooled to reduce electronic background. The screen thickness was chosen in such a way as to reduce light scattering in the screen while keeping a reasonable detective quantum efficiency. We refer the reader to a previous article for a more detailed description of a similar detector for lower energy (Koch, 1994).

In this first experiment the spatial resolution of the detection system was limited by scattering in the phosphor screen. We measured it to be approximately 50 µm. However, a better resolution should be achieved by improving the method of conversion of X-rays into visible light (Koch *et al.*, 1998). A schematic layout of the detector is shown in Fig. 2. The distance between the detector and

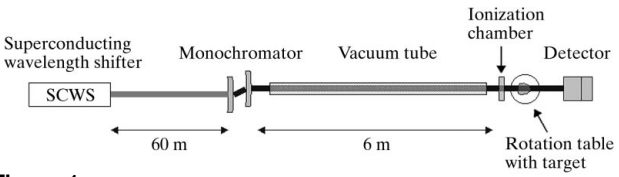

Figure 1
High-energy tomography set-up at beamline ID15A of the ESRF.

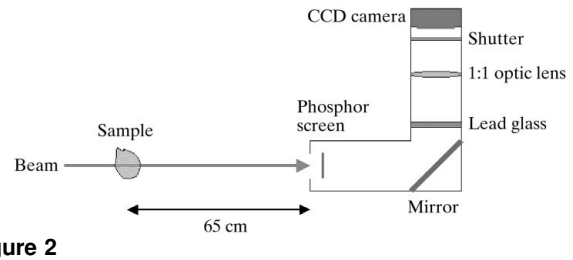

Figure 2
Schematic view of the position-sensitive detector developed to record high-energy X-rays.

the sample is small enough (65 cm) to neglect diffraction broadening. Indeed, this broadening, approximately equal to the radius of the first Fresnel zone (the square root of the product of this distance and the wavelength), is small, *i.e.* 2.6 μm, compared with the detector resolution. On the other hand, this distance is large enough to reduce effects due to Compton scattering. In the experiment, no appreciable effects due to Compton scattering in the sample were observed.

Various samples were scanned including artificial objects. All were chosen such that the uranium concentration, distribution and granularity were very different, allowing the assessment of the possibilities of the method. Due to this wide variety of samples, the CCD camera had to measure with exposure times ranging from 0.15 to 2 s. The quantity of data was also adapted to the structure of the sample, by binning the pixels of the CCD to record photons using 100×100 μm^2 or 50×50 μm^2 macro-pixels.

The procedure used during the experiments was to select the first photon energy, to position the sample out of the beam and to measure the incident-beam distribution, then to position the sample in the beam and to measure the attenuation for 200 different rotations of the sample, equally distributed over 180°. The samples being generally higher than the beam height, the scan was repeated for different vertical sample positions. After the whole sample was scanned, the beam energy was changed and the whole process repeated at the second energy. The incident-beam distribution was not uniform but the shape did not change with time. However, the average X-ray intensity decreased slowly with time, ∼9% in 1 h. Therefore an ionization chamber was used to normalize the data. Including the time to change energies, to rotate or move up the sample, and the time to read out and save the image (2–3 s), a typical double scan of a $2 \times 2 \times 2$ cm^3 sample took ∼2 h.

3. Data analysis

The quality of our data allowed us to analyse them using the filtered back-projection reconstruction technique. This is a well known method, used in different kinds of medical tomographies such as the classic computer tomography (CT), micro-CT, positron emission tomography *etc.* (Herman, 1980; Kak & Slaney, 1988; Parker, 1990). Because it is a direct method in contrast with iterative algorithms, it is also rather fast. On a PII-266 MHz PC, the reconstruction of a $2 \times 2 \times 2$ cm^3 sample takes ∼1.5 h.

A reconstruction and visualization package (Materna, 1999) was developed on *Labview*© and *Visual C++*© to analyse our data. It includes two ways to process the images. The first is to reconstruct separately the sample at the two energies and to subtract at the end the resulting three-dimensional distributions. An advantage of this method is that one obtains a useful comparison between the classic X-ray reconstruction and the element distribution. In the second, the ratio of the images at the two energies is used as input for the reconstruction; it yields directly the element distribution and, because the reconstruction is the slowest process, this way is about twice as fast. It should be noted that due to Beer's law the logarithm of the data has to be taken before using the reconstruction algorithm. This algorithm is linear; therefore, taking the ratio of two data sets (above and below the *K*-edge) before reconstruction is equivalent to subtracting at the end the two separately reconstructed images. The reconstruction algorithm has been already described in a previous paper (Materna *et al.*, 1999) for two-dimensional objects. Only minor modifications have been necessary to adapt the algorithm to this experiment. Indeed, the reconstruction of three-dimensional objects is made by processing successively horizontal slices of the object.

Finally, the reconstruction yields the three-dimensional matrix of the concentration of the element under study. It is then possible to view slices through the three-dimensional distribution or, using *IDL*©, to view 'iso-density' surfaces. The latter is useful to view the sample all at once; the former is best used to view details inside the sample.

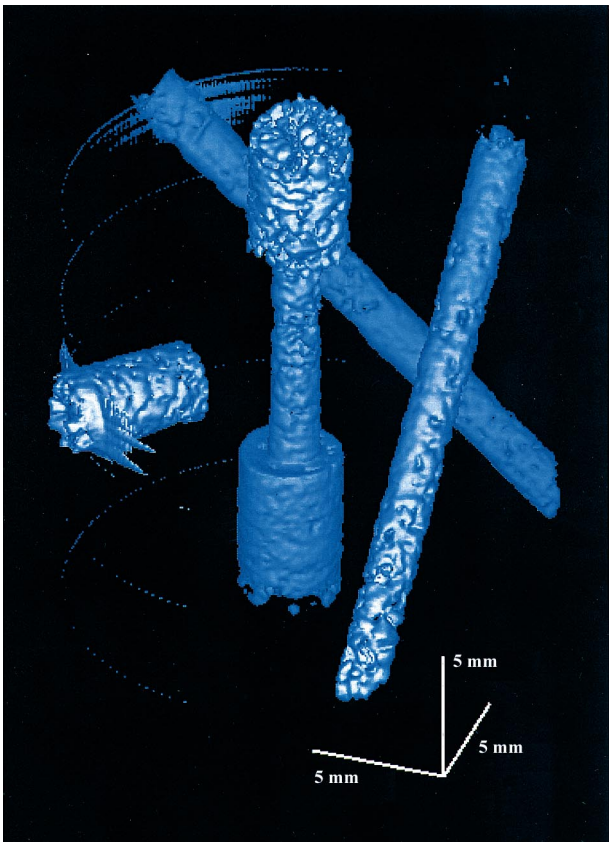

Figure 3
Three-dimensional reconstruction of the uranium content of an artificial sample. Several holes were drilled at different positions and with different angles in an aluminium cylinder. The holes were then filled with uranyl nitrate (the mean density of uranium in this powder equals 1 g cm^{-3}). Granules can be clearly observed in the upper less compressed part.

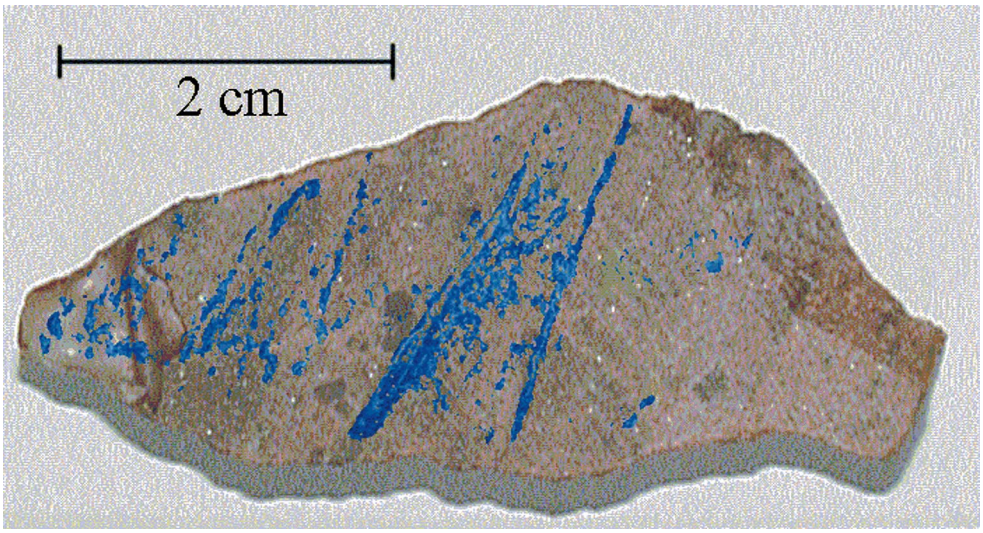

Figure 4
Three-dimensional reconstruction of the uranium distribution of a volcanic stone (in blue) superposed on the photograph of the same stone. It can be seen that the uranium settled preferentially in layers.

4. Results

To illustrate the possibility of distinguishing uranium with the *K*-edge tomography, a scan was performed for an artificial sample consisting of an aluminium cylinder with holes drilled at different positions and filled with uranyl nitrate powder. In the reconstruction, Fig. 3, the aluminium container is not perceptible; moreover, the uranium distribution even shows inhomogeneities produced during the filling of the holes.

A first application of this tomographic method is shown in Fig. 4. It consisted of detecting uranium in a volcanic rock from Newfoundland, Canada. The layered deposit of uranium can be precisely located and observed inside the stone. The same method was then used to study five small crystallites of autunite found in Tessin, Switzerland. All were placed together in an aluminium container to be scanned at the same time. In Fig. 5 we show the quality of the raw data for one out of the 200 projections. It illustrates also how only the uranium distribution remains after the ratio of the two radiographs is taken. Finally, as illustrated in Fig. 6, the distribution in a slice of the sample reveals the

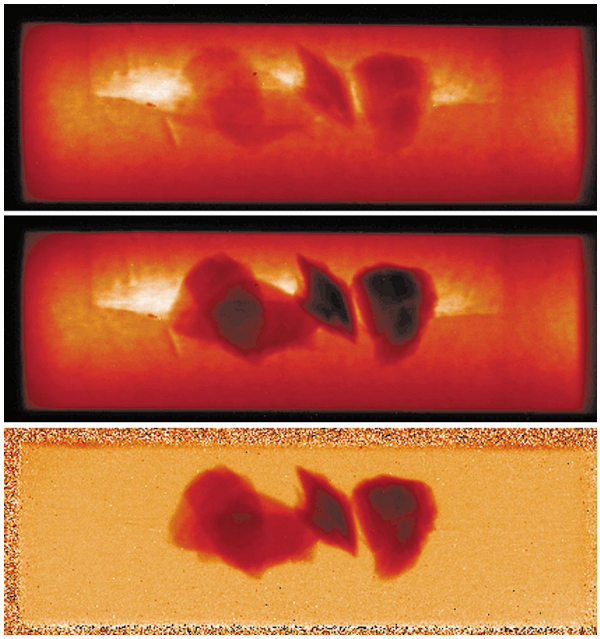

Figure 5
Radiographs of a sample containing five crystallites of autunite taken below (top) and above (middle) the *K*-edge of uranium. The lower part shows the ratio of the two images, each first normalized by the incident beam distribution. This ratio yields the uranium distribution.

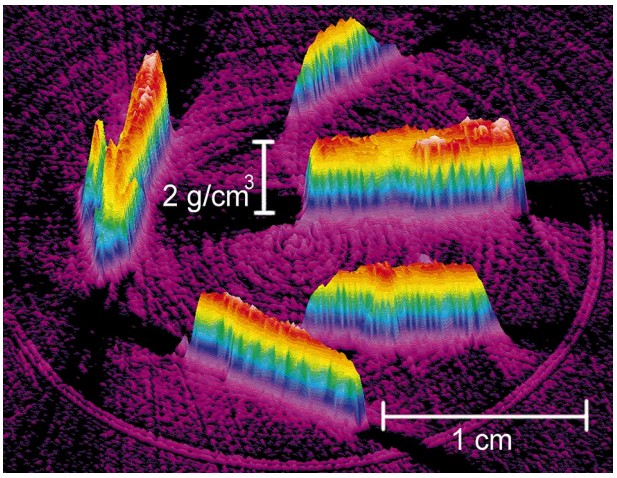

Figure 6
Three-dimensional graph of a slice of 50 μm through the sample from Fig. 5. The height is proportional to the uranium concentration.

inner uranium repartition in the crystallites. The uranium concentration was found to be $\sim$2 g cm^{-3}.

Another example of the possibilities of the method is the study of a stone containing pitchblende. This ore contains a large quantity of uranium oxide (U_3O_8) but the tomography shows that the compound neglects entire zones in the centre of the piece. This is illustrated in Fig. 7. The large number of artefacts is due to the high contrast in the absorption patterns between the inner part of the sample and the outside. This causes smoothing of the edges in the reconstruction of the sample. These effects could be avoided by using adequate masks (attenuation pieces) placed in the path of the photons, before the sample, in order to modify the photon distribution passing through the sample (Materna *et al.*, 2000).

For most of the samples we scanned, the sensitivity to detect uranium was limited by the dynamic range of the CCD camera and not by the intensity of the beam. Mostly the acquisition time of images was much shorter than the readout and saving time (a few hundreds of microseconds compared with at least 2 s). Thus, choosing a higher-dynamic-range CCD would allow imaging with longer acquisition time and thus improve the sensitivity at no time cost. The minimal uranium density that we could see with

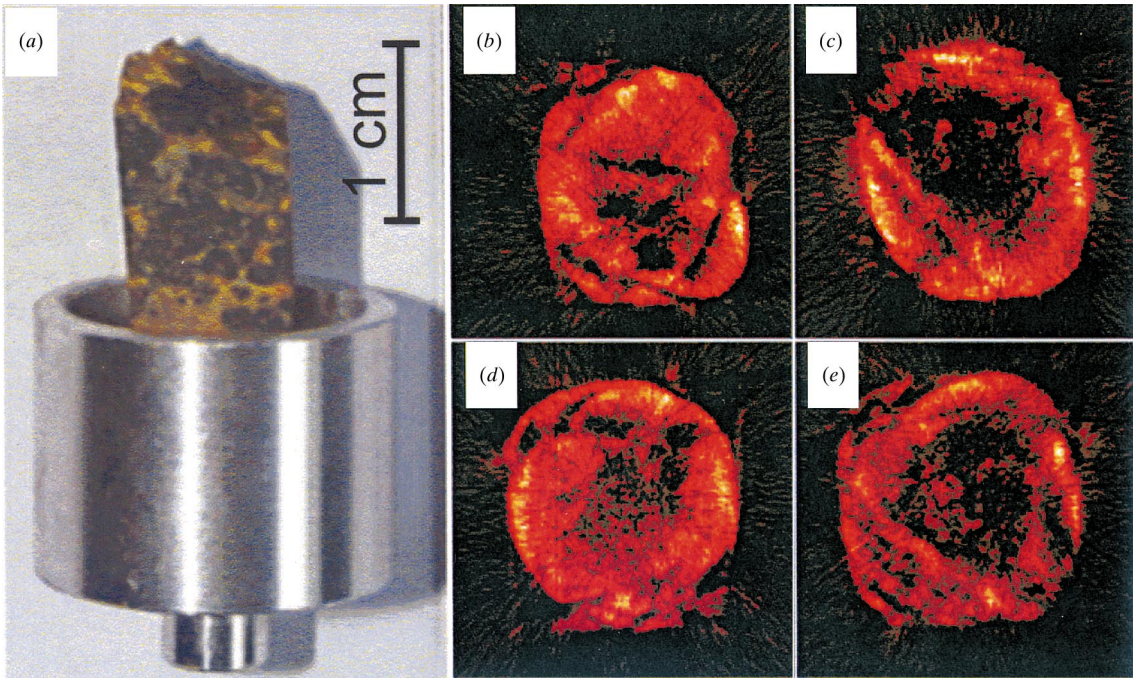

Figure 7
Tomographic reconstructions of a pitchblende stone (an ore containing essentially U_3O_8) showing that uranium is not uniformly spread and neglects entire zones inside the sample. (*a*) Photograph of the stone in its aluminium support as it was scanned at the ESRF beamline. (*b*)–(*e*) Four slices through the sample taken at different heights. The size of each slice is 12 $\times$ 12 $\times$ 0.1 mm^3.

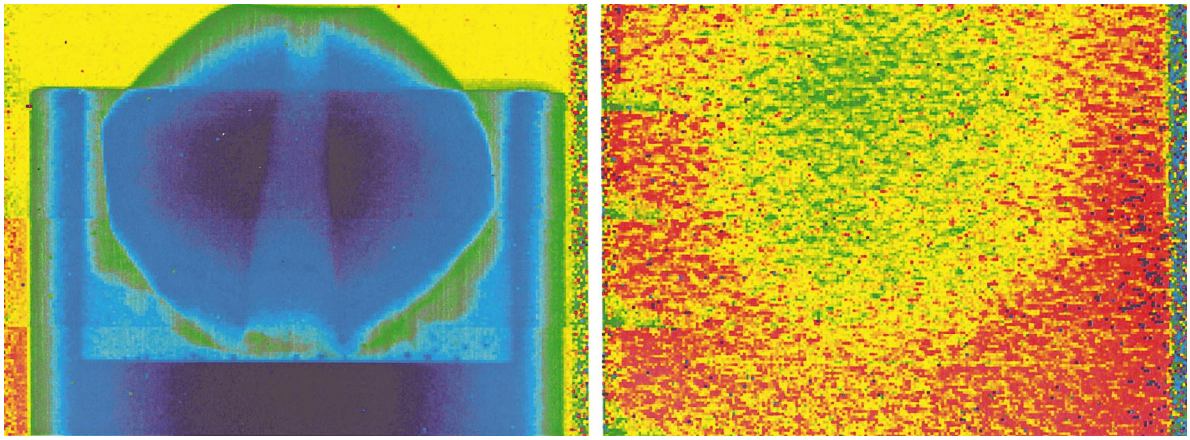

Figure 8
Left: radiograph at 116.6 keV of a sample with a pearl containing 0.33% uranium. Right: a signal is still visible in the dual energy result.

our set-up was of the order of 8 mg cm^{-3}. It was estimated by scanning a pearl containing 0.33% uranium, uniformly distributed. Fig. 8 illustrates the sample by two radiographs. The first was performed below the *K*-edge. The pearl and the aluminium holder both give the same attenuation. The second radiograph is the result of the dual energy subtraction. The aluminium holder disappears but there is still information on the uranium content in the pearl. This case corresponded to 1% attenuation by the sample. So the signal in the CCD just exceeded the background.

5. Conclusions and outlook

It was shown that the heaviest natural element could be visualized by element-sensitive tomography using synchrotron radiation. Important applications could lie in the study of diffusion processes of actinides, which are important for geology (Pb, Bi, Th, U), health physics (Rn) and nuclear waste storage (U, Ac, Pu). Other applications could be linked with studies on filters or coatings. With this first experiment at ESRF, we showed that *K*-edge tomography could be an impressive tool in the field of heavy-elements research. First, the high energies used permit scanning of quite thick (larger than 1 cm) and dense samples (uranium concentration higher than 1 g cm^{-3}) with a good resolution (50 μm). Then, the choice of a CCD camera as detection system allows fast scans with a good sensitivity (uranium concentration less than 0.01 g cm^{-3}). The scanning time was mainly limited by the readout time of the CCD. It is also several magnitudes shorter than the time required to scan a sample using our earlier set-up at Ghent (Materna *et al.*, 1999). Finally, the data analysis is fast enough to be performed during the experiment.

TM and JJ acknowledge financial support by the Swiss National Science Foundation, WM and BM from the Flemish Fund for Scientific Research, Flanders (Belgium) (FWO) and from the Research Board of Ghent University. We would like to thank Professor M. Maggetti and Dr H. Surbeck for lending us some of the samples.

References

Bertschy, M., Crittin, M., Jolie, J., Mondelaers, W. & Warr, N. (1995). *Nucl. Instrum. Methods*, B**103**, 330–338.
Bertschy, M., Jolie, J. & Mondelaers, W. (1996). *Appl. Phys.* A**62**, 437–443.
Bonse, U., Bush, F., Günnewig, O., Beckman, F., Delling, G., Hahn, M. & Kvick A. (1996). *ESRF Newsl.* **25**, 21–23.
Flannery, B., Deckman, H., Roberge, W. & D'Amico, K. (1987). *Science*, **237**, 1439–1444.
Fryar, J., McCarthy, K. J. & Fenelon, A. (1987). *Nucl. Instrum. Methods*, A**259**, 557–565.
Grodzins, L. (1983). *Nucl. Instrum. Methods*, **206**, 547–552.
Herman, G. T. (1980). *Image Reconstruction from Projections.* New York: Academic Press.
Kak, A. C. & Slaney, M. (1988). *Principles of Computerized Tomographic Imaging.* NewYork: IEEE Press.
Kinney, J. H., Haupt, D. L., Nichols, M. C., Breunig, T. M., Marshall, G. W. Jr & Marshall, S. J. (1994). *Nucl. Instrum. Methods*, A**347**, 480–486.
Koch, A. (1994). *Nucl. Instrum. Methods*, A**348**, 654–658.
Koch, A., Raven, C., Spanne, P. & Snigirev, A. (1998). *J. Opt. Soc. Am.* A**15**, 1940–1951.
Lewis, R. (1997). *Phys. Med. Biol.* **42**, 1213–1243.
Materna, Th. (1999). *TOUPI. A Reconstruction and Visualization Package.* Internal report IPF-PAN. University of Fribourg, Switzerland.
Materna, Th., Baechler, S., Jolie, J., Stritt, N., Mondelaers, W., Masschaele, B., Cauwels, P., Tschentscher, Th., Honkimäki, V. & Johner, H. U. (2000). In preparation.
Materna, Th., Jolie, J. & Mondelaers, W. (1999). *Nucl. Instrum. Methods*, B**149**, 141–146.
Nave, C., Clark, G., Gonzalez, A., McSweeney, S., Hart, M. & Cummings, S. (1995). *J. Synchrotron Rad.* **2**, 292–295.
Parker, J. A. (1990). *Image Reconstruction in Radiology.* Boston: CRC Press.
Snigirev, A., Snigireva, I., Kohn, V., Kuznetsof, S. & Schelokov, I. (1995). *Rev. Sci. Instrum.* **66**, 5486–5492.
Tschentscher, Th. & Suortti, P. (1998). *J. Synchrotron Rad.* **5**, 286–292.